

Morphological properties of galaxies in different Local Volume environments

I.D. Karachentsev^{1*}, E.I. Kaisina¹ and D.I. Makarov¹

¹ *Special Astrophysical Observatory of the Russian Academy of Sciences, Nizhny Arkhyz, Karachai-Cherkessian Republic*

Accepted XXX. Received YYY; in original form ZZZ

ABSTRACT

We consider an all-sky sample of 1029 Local Volume (LV) galaxies situated within a distance of 11 Mpc. Their majority have precise distances, estimates of hydrogen mass fraction and star-formation rate derived from far-ultraviolet or H α fluxes. To describe an environment, we attribute two dimensionless values: the density contrast created by the most significant neighbour and the local density contrast produced by all neighbours within a separation of 1 Mpc. The hydrogen mass fraction exhibits a weak effect of H I deficiency being the most pronounced for dwarf irregular galaxies. The specific star-formation rate (sSFR) is more sensitive to the environment than the hydrogen mass fraction. Almost all (99 per cent) LV galaxies have their sSFR below -9.4 dex (yr^{-1}). We notice that irregular dwarfs as well as late-type bulgeless galaxies are capable to reproduce their stellar mass with the observed sSFR over the cosmic time. Thus, the transformation of gas into stars in dIrs and spiral disks is rather sluggish unlike that in E, S0, dSph galaxies, whose star-formation history has been stormy and short. Scatter of SFR(H α)-to-SFR(FUV) ratio increases from Sc, Sd, Sm galaxies towards BCD, Im, Ir types that favours the idea of bursty star formations in low-mass galaxies. However, this bursty activity is caused rather by internal processes than by an external tidal action. A fraction of quenched E, S0, dSph galaxies increases from ~ 5 per cent in the field up to ~ 50 per cent in the densest regions.

Key words: galaxies: formation – galaxies: dwarf – galaxies: star formation

1 INTRODUCTION

The Λ CDM standard cosmological model effectively explains the origin and evolution of the large-scale structure of the Universe. However, with transition to ≤ 1 -Mpc scales, predictions of the standard model begin to diverge from observation data. One of the most well-known discrepancies is the observed shortage (dozens of times!) of a number of dwarf companions around normal-mass galaxies as compared with the results of numerical modelling in the framework of Λ CDM (Moore et al. 1999, Klypin et al. 1999).

To test numerical models, one needs a sample of galaxies limited by their distance rather than flux (apparent magnitude). The difference between two kinds of galaxy selection is enormous, e.g., the famous Revised Shapley-Ames Catalog (Sandage & Tammann 1981) with 1246 brightest galaxies and a catalogue of 1000 nearest galaxies overlap by 8 per cent only. According to Peebles (1993), compiling a representative sample of nearby galaxies located within a fixed distance is an important task for observational cosmology on small scales.

The global properties of galaxies, such as atomic hydrogen abundance or star-formation rate, have been considered by many authors (Huang et al. 2012, Karachentsev & Kaisina 2013, Knobel et al. 2015, Knapen et al. 2015, Beygu et al. 2016, Watkins et al. 2017) using samples of different composition and depth. However, from our point of view, a representative sample of the nearest galaxies has an undeniable advantage over the others in this respect, since various effects of observational selection in it are easier to analyse and account for.

There is extensive literature on the dependence of integrated parameters of gaseous and stellar components of galaxies on the density of their environments. In recent years, different scenarios of transformation of gas into stars in galaxy disks and bulges were discussed by Birrer et al. (2014), Schawinski et al. (2014), Pipino et al. (2015), Rodriguez-Puebla et al. (2017), Semenov et al. (2017), Barsanti et al. (2018). According to many data, the process of morphological evolution of a galaxy essentially depends on its baryon mass which increases with time as galaxies occasionally merge. However, it remains unclear what the role of diffuse intergalactic medium is in the global evolution of normal and dwarf galaxies. In accordance with predictions

* ikar@sao.ru

of the standard cosmological model, the basic amount of cosmic baryons is distributed outside optical borders of galaxies as warm plasma, the large-scale structure and temperature of which is still the target of speculations. Systematic analysis of observation data on galaxies in the reference sample of the Local Volume can facilitate a solution of the issue specified.

2 THE LOCAL VOLUME SAMPLE

The first step to create a distance-limited sample of nearby galaxies was made by Kraan-Korteweg & Tammann (1979), who compiled a list of 179 galaxies with expected distances within 10 Mpc. Later, Karachentsev (1994) and Karachentsev et al. (2004) expanded this list up to 226 and 450 galaxies, respectively. The latest version of the ‘Updated Nearby Galaxy Catalog’ (Karachentsev et al. 2013) contains 869 galaxies with distance estimates $D < 11$ Mpc.

In recent years, due to wide-field sky surveys in the optical range and in the H I 21-cm line, the number of catalogued galaxies in the Local Volume (LV) with $D < 11$ Mpc significantly increased, and for January 2018 it exceeded a thousand. The LV database¹ contains different properties of nearby galaxies and atlas of their images (Kaisina et al. 2012). Galaxies have been included in the LV sample by one of two conditions: a) the radial velocity of a galaxy in reference to the Local Group (LG) centroid is $V_{LG} < 600$ km s⁻¹ or b) the estimate of its distance with any method is $D < 11$ Mpc. For ~ 400 LV galaxies, distances were measured with an accuracy of (5–10) per cent at the Hubble Space Telescope (HST) from the tip of the red-giant branch (TRGB).

Currently, for most LV galaxies hydrogen masses are determined and star-formation rates (SFR) are estimated by the flux in the far ultraviolet (FUV), measured at the GALEX satellite, or in the H α emission line. Table 1 presents numbers of the LV galaxies observed in H I, FUV and H α line as well as numbers of detected objects among them. Here we reduced the total number of LV galaxies from 1153 to 1029, omitting 28 galaxies with strong Galactic extinction $A_B > 3.0$ mag according to Schlafly & Finkbeiner (2011) and 98 galaxies which have been selected according to their low velocity $V_{LG} < 600$ km s⁻¹ but whose distance estimates turn out then to be beyond 11 Mpc. The first row of Table 1 indicates numbers of the LV galaxies belonging to different morphological types on de Vaucouleurs scale: $T = 10$ (Ir), $T = 9$ (Im, BCD), $T = 8 - 6$ (Sm, Sdm, Sd, Sdc), $T = 5 - 1$ (Sc, Sbc, Sb, Sab, Sa) and $T < 1$ (E, S0, dE, dSph).

Appendix provides basic observation data on 1029 LV galaxies used in our analysis. The full machine-readable version of the list is available at the Vizier database². Individual references to original sources of the data can be found in the LV database.

Abundant observables for this sample covering the stellar-mass range of ~ 7 dex and minimally burdened with selection effects allows one to study different properties of

galaxies depending on the environment in the wide range of local densities (~ 5 dex within a sphere of the 1 Mpc radius).

3 INDICATORS OF ENVIRONMENT DENSITY IN THE LOCAL VOLUME

In the vicinity of every LV galaxy, there are numerous neighbours ‘n’ with masses M_n at spatial separations D_n . Due to enormous difference between galaxies by masses, the term ‘the nearest neighbour’ loses its physical meaning; instead, the notion ‘the most significant neighbour’ is advisable, the tidal force of which $F_n \sim M_n/D_n^3$ prevails the gravitational influence of other neighbours. We characterized each LV galaxy with the tidal index

$$\Theta_1 = \max[\log(M_n/D_n^3)] + C, n = 1, 2, \dots, N,$$

where the parameter $C = -10.96$ was chosen so that a galaxy with $\Theta_1 = 0$ was located on the ‘zero-velocity sphere’ relative to its most significant neighbour, i.e., the Main Disturber (MD). In other words, a galaxy with $\Theta_1 < 0$ was considered a ‘field galaxy’ causally unrelated to its MD, as the crossing time for this pair exceeds the age of the Universe.

However, the MD position could considerably vary with time owing to orbital motion, thus, we also used another, more robust, local-density indicator

$$\Theta_5 = \log\left(\sum_{n=1}^5 M_n/D_n^3\right) + C,$$

which accounted for contribution of five most significant neighbours to density contrast. The C parameter here is the same as in the case of Θ_1 .

Finally, we have calculated the third indicator for each LV galaxy

$$\Theta_j = \log[j_K(1 \text{ Mpc})/\langle j_K \rangle],$$

where $j_K(1 \text{ Mpc})$ denotes the average density of galaxy luminosity in the K-band within a 1 Mpc radius and $\langle j_K \rangle = 4.28 \times 10^8 L_\odot/\text{Mpc}^3$ (Jones et al. 2006) is the mean global density of the K-luminosity at the Hubble parameter $H_0 = 73$ km s⁻¹ Mpc⁻¹. In so doing, the luminosity of the central galaxy itself was not taken into account. If a galaxy had no neighbours within the 1 Mpc radius, its dimensionless parameter Θ_j was assumed equal to -3.5 .

Hereinafter, we assume that the stellar mass of a galaxy is expressed through its luminosity in the K-band as

$$M_* = 1(M_\odot/L_\odot) \times L_K$$

according to Bell et al. (2003). More recent estimates of the proportionality factor yield its value closer to $0.5(M_\odot/L_\odot)$ (McGaugh & Schombert 2014, Pomonareva et al. 2018) which should be kept in mind when normalizing the hydrogen mass M_{HI} and the star-formation rate SFR per unit M_* . The main source of data on K-band magnitudes is the 2MASS Sky Survey (Jarrett et al. 2000, 2003) supplemented by photometric measurements from (Fingerhut et al. 2010, Vaduvescu et al. 2006). At the lack of accurate photometry, K-magnitude was determined via apparent B-magnitude and morphological type T by a relation (Jarrett et al. 2003): $\langle B - K \rangle = 4.10$ for $T < 3$, $\langle B - K \rangle = 2.35$ for $T > 8$,

¹ <http://www.sao.ru/lv/lvgdb>

² <http://edsarc.u-strasbg.fr/viz-bin/qcaJ/other/>

and $\langle B - K \rangle = 4.60 - 0.25T$ for intermediate types $T = 3 - 8$ by de Vaucouleurs scale.

The upper and lower panels in Fig. 1 show the relation between three tidal indices: Θ_1 and Θ_5 , Θ_1 and Θ_j for 1029 LV galaxies. As we can see, density variations determined by tidal indices Θ_1 and Θ_5 reach nine orders. Both the indices are closely correlated. The density excess ($\Theta_5 - \Theta_1$) does not exceed 0.6 dex even in the most extreme cases. Therefore, further we do not use the parameter Θ_5 in analysing various properties of LV galaxies.

As follows from the bottom panel of Fig. 1, the tidal index Θ_1 and local density contrast Θ_j are also correlated, although, the statistical relation between them looks less clear and nonlinear. The dispersion Θ_1 grows with the increase of Θ_j . The local-density range in a sphere of the 1 Mpc radius exceeds 5 dex. To estimate specific features of this diagram, let us consider an extreme case of the ultra-compact companion SUCD1 (Hau et al. 2009) near the giant galaxy NGC 4594 = M104 = Sombrero. Physical connection of galaxies is confirmed by their radial velocities: 1109 km s^{-1} and 894 km s^{-1} , respectively. The companion SUCD1 is located at a projected distance of $2.7'$ from the center of Sombrero, which, with the TRGB distance of Sombrero of 9.55 Mpc (McQuinn et al. 2016), corresponds to 7.4 kpc. The tidal index Θ_1 for SUCD1 is calculated on the assumption of that the companion is located at the same distance as the giant galaxy. If the distance to SUCD1 was measured with the TRGB method with the 5 per cent accuracy, then this would fix the mutual distance of two galaxies along the line of sight with an accuracy of ± 480 kpc. With such a separation shift by 480 kpc, the tidal index $\Theta_1 = 6.7$ could decrease to 1.3. From this example, we deduce that a considerable part of the scatter of galaxies along the Θ_1 axis is probably due to measurement errors of their distances. Nevertheless, we preserve both parameters for further analysis: Θ_1 and Θ_j , giving a preference to the parameter Θ_1 as more sensitive to SFR bursts and gas depletion in dwarf galaxies than the density contrast Θ_j in the 1 Mpc radius sphere.

4 GASEOUS FRACTION OF MASS VS. LOCAL DENSITY

The atomic hydrogen mass M_{HI} of a galaxy determined from its flux in the HI line as

$$(M_{\text{HI}}/M_{\odot}) = 2.356 \times 10^5 \times D^2 \times F_{\text{HI}}$$

is a parameter quite sensitive to the environment. Here D is in Mpc and the flux F_{HI} is in Jy km s^{-1} . The effect of the HI deficiency in spiral galaxies situated in groups and clusters was studied by Haynes & Giovanelli (1984) in detail. The sweeping-out of gas from galaxy disks during their motion through a dense virial core is assumed to be the main mechanism of formation of the HI deficiency. Obviously, the sweeping-out of gas from dwarf galaxies happens easier due to a shallow potential well as compared to disks of massive galaxies. Since the hydrogen mass correlates with the stellar mass of a galaxy and with its morphological type, then in order to reduce a scatter of data in diagrams, we consider the ratio M_{HI}/M_* for each morphological type separately. An additional advantage arises under such an approach, as

the ratio M_{HI}/M_* does not depend on errors of a galaxy distance.

Major sources of data on HI fluxes of nearby galaxies are ‘blind’ surveys of wide areas of sky with the radio telescopes: Parkes, HIPASS (Koribalski et al. 2004), Arecibo, ALFALFA (Haynes et al. 2011) and Westerbork, WSRT-CVn (Kovac et al. 2009). Special observations of several hundred candidates to nearby dwarfs have been performed by Huchtmeier et al. (2000) at the 100-m dish in Effelsberg. The data of second and third rows of Table 1 show that HI fluxes are measured now for 794 objects among 1029 LV galaxies, but 210 of them have only upper limits of the flux. Unfortunately, a considerable area of the northern sky is still uncovered by a systematic HI-survey.

Distributions of the LV galaxies with their hydrogen-to-stellar mass ratio depending on the tidal indices Θ_1 and Θ_j are presented in a set of panels in Fig. 2, Fig. 3 and Fig. 4. A typical uncertainty of the HI-mass fraction on the Figures is (0.1 - 0.2) dex. The galaxies with only upper limit of HI-flux are shown by open circles. For each morphological category, we calculated the linear-regression parameters $Y = a + bX$, the data on which are given in the upper part of Table 2. Here and so on, galaxies with upper limit of their HI, FUV or H α fluxes were ignored. The Table contains regression parameters for both the tidal indices: Θ_1 and Θ_j . The cases with a slope significant at the 3-sigma level are highlighted in Table 2 by boldface. Considering the data of the Figures and Table 2, we notice the following features and trends.

4.1 Dwarf irregular galaxies (T = 10)

Despite the fact that irregular galaxies are assigned to one and the same type, $T = 10$, they show a great scatter of the hydrogen-to-stellar mass ratio. Some dIr objects: ESO 215-009, And IV, with $M_{\text{HI}}/M_* > 10$ have served as targets of a detailed study (Warren et al. 2004, Karachentsev et al. 2016). Both the gas-rich galaxies are isolated. However, the high ratio $M_{\text{HI}}/M_* \simeq 15$ in another dwarf system, BK3N near M 81, seems to be caused by entangling HI fluxes from these galaxies being in contact in the sky. It should be also noted that some low-surface-brightness dwarfs (e.g., HS 117) are referred to the dIr type ($T = 10$), but they look like transitional (Tr) between dIr and dSph by their smooth structure, reddish colour, and low hydrogen abundance.

On the whole, the dIr population demonstrates the decreasing ratio M_{HI}/M_* with the increase of the parameters Θ_1 and Θ_j . This effect is more prominent ($b = -0.060 \pm 0.021$) in the case of tidal index Θ_1 that points on the primary role of the most significant neighbour (MD) in the process of gas evacuation from its dwarf companions.

As seen from Table 1, about 11 per cent of dIr galaxies observed in HI have only an upper limit of their HI flux (denoted with open circles in Fig. 2). Most of them are close companions to massive spirals having parameters $\Theta_1 > 1$ and $\Theta_j > 1.5$. Taking these galaxies into account would make the regression-line slope steeper.

The average hydrogen-to-stellar mass ratio in a population of irregular dwarfs is close to unity, i.e. they are in a half-way of their evolution. The mean difference in $\log(M_{\text{HI}}/M_*)$ from field galaxies to group members reaches 0.3 dex which is smaller than the dispersion of this ratio, $\sigma[\log(M_{\text{HI}}/M_*)] \simeq 0.48$. Consequently, the environment

density is not the basic factor determining the observed gas-to-stars fraction in irregular dwarfs.

4.2 Magellanic and Blue Compact Dwarfs ($T = 9$)

As seen from Table 2, the average stellar mass of these dwarfs is about 5 times greater than that of dIrs, and the M_{HI}/M_* ratio is on average 2.5 times lower. The H I-deficiency effect as a function of Θ_1 or Θ_j is manifested as only a weak tendency with the regression line slope being within its statistical error.

The bright satellites of our Galaxy: the Large (LMC) and Small (SMC) Magellanic clouds, look like typical representatives of this population of dwarfs. Wherein, there are examples of objects with the greater (AGC 112454) and very small (DDO 082) H I-abundance.

4.3 Bulgeless disks ($T = 8 - 6$)

The last column in Table 2 shows that the typical stellar mass of late-type spirals in the Local Volume, $\langle \log M_* \rangle = 9.14$, is much greater than that of irregular (7.46) and Magellanic (8.21) dwarfs. With the increase of the environment density, the H I-deficiency effect is seen only as an insignificant tendency ($b = -0.02 \pm 0.02$) of the expected sign. All 130 LV galaxies of these morphological types are detected in H I. Relative abundance of hydrogen in them is almost the same (-0.46 dex) as that in BCD and Im dwarfs.

4.4 Early-type spirals ($T = 5 - 1$)

Galaxies of the Sc, Sb, and Sa types are inconsiderable in number in the Local Volume ($N = 29$). All of them are detected in H I. Their average stellar mass is 10.63 dex, and the average hydrogen-to-stellar mass ratio is only -1.44 dex. The M_{HI}/M_* ratio does not reveal any correlation with the environment parameters Θ_1 and Θ_j .

4.5 E + S0 + dSph galaxies ($T < 1$)

In this mixed sample of objects with old stellar population, dwarf spheroidal galaxies predominate in number. Current H I-surveys are too shallow to reliably measure their H I flux. As one can see from Table 1, in 93 per cent of cases (shown in bottom panel of Fig.4 by open circles), there was detected only the upper limit of H I-flux. Most galaxies of this type are concentrated in high-density regions. In this regard, a specific selection effect arises: angular separations between spheroidal dwarfs and their massive neighbour are comparable to a beam size of radio telescopes which makes it difficult to measure the H I flux from tight dwarf companions.

5 STAR-FORMATION RATE VS. LOCAL DENSITY

Following Lee et al. (2009, 2011), we determined the integrated star-formation rate of a galaxy in units of (M_\odot/yr) as

$$\log(\text{SFR}) = 2.78 + 2 \log D - 0.4 \times m_{\text{FUV}}^c,$$

where the distance D is expressed in Mpc and the apparent magnitude of a galaxy in the far ultraviolet, m_{FUV}^c , is measured at the GALEX satellite (Gil de Paz et al. 2007) and corrected for Galactic and internal extinction. As it is shown in Table 1, the GALEX survey yields FUV fluxes for 647 LV galaxies and also flux upper-limits for other 230 galaxies.

In order to avoid errors of distance measurements and reduce the statistical scatter, we used the specific star-formation rate normalized to stellar mass of a galaxy

$$\text{sSFR} = \text{SFR}/M_*.$$

Figs. 5–7 present the distribution of LV galaxies over the specific star-formation rate and the environment-density indicators. A typical error of sSFR on them is $(0.1 - 0.2)$ dex. Galaxies were divided into morphological types in the same manner as in the previous section. The middle part of Table 2 shows the linear-regression parameters for each subsample. Based on these data, we can notice the following tendencies.

5.1 Dwarf irregular galaxies

Among 339 LV dIr galaxies within the GALEX survey area, the FUV flux was detected in 301 objects, i.e., in almost 90 per cent of the sample. Their average star-formation rate is

$$\langle \log(\text{sSFR}) \rangle = -10.24(\text{yr}^{-1}).$$

Consequently, with such a star-formation rate, being permanent throughout the age of the Universe, $T_0 = 10.14$ dex (yr), a typical irregular dwarf is able to reproduce 80 per cent of its stellar mass. (Note that assuming the ratio $M_* = 0.5(M_\odot/L_\odot) \times L_K$ by McGaugh & Schombert (2014) would yield the average star-formation rate for dIrs to be slightly higher in past than in the present epoch).

Passing from isolated irregular galaxies into group members, the average star-formation rate 3–4 times drops. This effect appears significant at the level of 4–5 sigma both by the parameter Θ_1 with the regression slope of $b = -0.089 \pm 0.018$ and Θ_j with its slope of $b = -0.076 \pm 0.017$. Consequently, the presence of a massive neighbouring galaxy does not intensify, yet on average diminishes the star-formation rate of its dwarf companions. This statement agrees with the result obtained earlier by Karachentsev et al. (2014) but disagrees with conclusions derived by Ellison et al. 2008, Di Mateo et al. 2008, Lelli et al. 2014 and Knapen et al. 2015. In particular, Knapen et al. 2015 investigated the influence of interactions on the star formation by studying a sample of 1478 nearby galaxies, all within a distance of 45 Mpc, and explored distribution of their sSFR with morphological type and with stellar mass. They found that sSFR is enhanced statistically in interacting galaxies. The increase is, however, moderate, reaching a maximum of a factor of 1.9 for the highest degree of interaction (i.e. mergers). A probable reason of the disagreement can be caused by different approaches to the sample selection. Knapen et al. 2015 selected preferably bright and large galaxies, while our LV sample consists of mainly low-mass galaxies exposed to quenching action of a massive neighbor.

The distribution of irregular dwarfs by sSFR does not show a distinct lower limit. Here one should also take into consideration that a part of the dIr population only have the upper estimate of their FUV flux. Furthermore, a number of dIrs (by our estimation, 40–50 per cent) have transitioned

into the quenched dwarf spheroidal category for the time T_0 . Along with this, a distinctive feature of this distribution is the presence of sharp upper limit $(\text{sSFR})_{\text{max}} \simeq -9.4$ dex that has been already noticed by (Karachentsev & Kaisina 2013). The presence of the upper limit can be also seen in observational data by Knapen et al. (2015), Pan et al. (2018), and in model calculations by Birrer et al. (2014). In our sample, there are only three irregular dwarfs near and slightly above this limit, the most outstanding of which is NGC 1592 with its $\text{sSFR} = -9.15$ dex. This isolated peculiar object looks like a chain of blue knots embedded in a faint envelope. Judging by a low color index $B - K = 1.55$ of NGC 1592, its K-luminosity from 2MASS survey (Jarrett et al. 2000, 2003), and accordingly the stellar mass, seems to be about two times underestimated. Accounting for this correction drops NGC 1592 below the specified limit which presence we consider as important characteristic of the star-formation process in the current epoch.

5.2 BCD and Im dwarfs

Among 120 galaxies of this sample within the area of GALEX survey, only one object is undetected in the FUV band. The average star-formation rate of the BCD + Im dwarfs,

$$\langle \log(\text{sSFR}) \rangle = -10.21 (\text{yr}^{-1}),$$

is almost the same as that of irregular dwarfs. However, their sSFR dispersion (0.38) is appreciably smaller than that in the previous sample (0.49). These more massive dwarfs also show the effect of SFR decrease with the increase of the environment density, although, their regression slope is somewhat smaller: $b = -0.105 \pm 0.033$ for the parameter Θ_1 and $b = -0.072 \pm 0.021$ for Θ_j .

Only one BCD dwarf, Mrk 36 = Haro 4, lies slightly above the limit $(\text{sSFR})_{\text{max}} = -9.4$ dex. Probably, this moderately isolated object is in a short-term phase of burst activity, the cause of which, however, is not due to interaction with neighbours.

5.3 Bulgeless disks

FUV fluxes are detected in all 118 late-type spiral galaxies observed with GALEX. Their average specific star-formation rate $\langle \log(\text{sSFR}) \rangle = -10.14$ (yr^{-1}) just coincides with the Hubble parameter, $\log(H_0) = -10.14$ (yr^{-1}). The star-formation rate in these galaxies is almost insensitive to the environment density. One can state that bulgeless galaxy disks have a uniform internal mechanism for converting gas into stars which works with remarkable consistency throughout the whole cosmological timescale $T_0 = H_0^{-1}$.

5.4 Early-type spirals

Representatives of this small subsample of LV galaxies significantly differ from each other in the disk-to-bulge mass ratio. For example, a disk is dominant in NGC 24, while in NGC 2787 and NGC 4594 (Sombrero) the main stellar mass is concentrated in their bulges. The GALEX survey detects the FUV flux in all 27 early-type spiral galaxies. However, the average specific star-formation rate for them,

$\langle \log(\text{sSFR}) \rangle = -10.95$, is about six times lower than that for late-type spirals, since the old quenched population of bulges is involved in normalization per unit of the galaxy's stellar mass. As was noticed by Abramson et al. 2014, normalizing to the mass of a disk itself, rather than to the total stellar galaxy mass, significantly reduces the dispersion of specific star-formation rates.

5.5 Quenched E, S0, and dSph galaxies

As seen from Table 1, the depth of GALEX survey is too shallow to draw reliable conclusions about specific features of star formation in galaxies with an old stellar population. FUV fluxes are measured for only 82 of 273 LV galaxies of these types. As a rule, these are the nearest galaxies like M 32 and NGC 205. Also, angular sizes for some dSphs in the Local Group (Fornax, Sculptor) are so large that estimation of their FUV flux can only be the upper limit due to abundant background objects falling into the galaxy borders.

The sSFR dispersion of the detected E, S0, and dSph galaxies is much greater than that of other types. The decreasing tendency of the star-formation rate of them with the increase of their environment density is weak. The average current star-formation rate for these galaxies is -12.23 dex (yr^{-1}) which is smaller than the H_0 cosmological scale by two orders of magnitude. According to Pipino et al. (2013), the global cosmic evolution of SFR as a function of a redshift Z splits into two different modes: a short epoch of intense star formation in E, S0, and dSph galaxies, as well in bulges of Sa-Sb galaxies before $Z = 2$, and a stage of slow conversion of gas into stars in disks of late-type galaxies extended over the whole cosmic time T_0 . This scenario quite agrees with observation data presented here for the LV galaxies.

6 STAR FORMATION AS SEEN IN FUV AND $H\alpha$ SURVEYS

Determination of SFR from the FUV flux corresponds to a characteristic timescale of ~ 100 Myr. Another method uses the integrated flux from a galaxy in the $H\alpha$ emission line. According to Kennicutt (1998),

$$\text{SFR} = 0.945 \times 10^9 \times D^2 \times F_c(H\alpha),$$

where the distance D is expressed in Mpc and the flux in $H\alpha$ in the units $[\text{erg} \times \text{cm}^{-2} \times \text{s}^{-1}]$ is corrected for the Galactic (Schlafly & Finkbeiner 2011) and internal extinction. This estimate characterizes the star-formation rate on a scale of ~ 10 Myr. Thus, the ratio $\text{SFR}(H\alpha)/\text{SFR}(\text{FUV})$ may be used to identify objects that are in a loud or quiet phases of their star-formation activity.

There are 573 galaxies in our sample with the estimated $\text{SFR}(H\alpha)$. Most of them (486) have the star-formation rate determined also via their FUV flux. The majority of $H\alpha$ -flux measurements were performed at the 6-m SAO RAS telescope with a typical error of ~ 0.07 dex (see Kaisin & Karachentsev 2014 and references therein).

The distribution of LV galaxies by the $\text{SFR}(H\alpha)/\text{SFR}(\text{FUV})$ ratio and the environment-density indicator Θ_1 is given in the panels of Figs. 8. Objects with

the upper limits for the $F(H\alpha)$ and $F(FUV)$ fluxes are represented by point-down or point-up triangles, respectively. Galaxies are divided by morphological type in the same manner as before. Linear-regression parameters for them are shown at the bottom of Table 2. Considering these data, we can draw the following tendencies:

a) The average value of $\log [SFR(H\alpha)/SFR(FUV)]$ monotonously increases along the Hubble sequence from $T = 10$ to $T = 1$. The amplitude of this variation reaches a value of 0.52 dex.

b) The smallest scatter of $SFR(H\alpha)/SFR(FUV)$ ratio is characteristic of late-type bulgeless spiral galaxies ($T = 8-6$).

c) The trends of the $SFR(H\alpha)/SFR(FUV)$ versus environment density look indistinct for galaxies of all types. Only in the case of E, S0, dSph- galaxies, the ratio decreases from isolated galaxies to group members with the slope $b = -0.268 \pm 0.085$ significant at the 3-sigma level.

Note that among extreme deviations of $SFR(H\alpha)/SFR(FUV) > 10$ there are both the cases of a galaxy being in the short-term phase of burst activity (M 82) and also the cases of erroneous overestimation of the $H\alpha$ flux: NGC 6503-d1 (Koda et al. 2015), JKB83 (James et al. 2017). On the other side, galaxies with $SFR(H\alpha)/SFR(FUV) < 1/10$, for example, KDG 52 and DDO 120, are apparently at a calm stage between bursts.

Sperello di Serego Alighieri has drawn our attention to the fact that neutral hydrogen in galaxies can be ionized not only by young stars but also by hot evolved stars. Therefore, in galaxies, where the old stellar population is dominant, the $H\alpha$ flux is not closely related to the star-formation process (Trinchieri & de Serego Alighieri 1991, Binette et al. 1994). Accounting for this factor is able to explain the high $SFR(H\alpha)/SFR(FUV)$ ratio which occurs for the E, S0 galaxies like NGC 4600 and for bulges of the S0a galaxies like NGC 3593.

Variations of the $SFR(H\alpha)/SFR(FUV)$ ratio depending on the $SFR(FUV)$ value, or galaxy mass, or morphological type were discussed by many authors (Lee et al. 2009, Meurer et al. 2009, Hunter et al. 2010, Fumagalli et al. 2011, Weisz et al. 2012, Karachentsev & Kaisina 2013, Lee et al. 2016, Watkins et al. 2017, Shimakawa et al. 2017). Pflamm-Altenburg et al. (2007, 2009) noticed that the observed systematic decrease of $SFR(H\alpha)$ relative to $SFR(FUV)$ from massive galaxies towards dwarfs could be caused by underestimating SFR via the $H\alpha$ flux due to shortage of the brightest young stars in dwarf galaxies. Fumagalli et al. (2011) and Weisz et al. (2012) suppose that the reason for this difference is mainly the bursty character of star formation in low-mass dwarfs.

The panels of Fig. 9 show the $SFR(H\alpha)/SFR(FUV)$ ratio as the stellar-mass function for various morphological types. Linear-regression parameters for them are shown at the bottom of Table 2. As seen from these data, the average value of $\log M_*$ grows along the Hubble sequence from $T = 10$ to $T = 5-1$ by three orders of magnitude. With the increase of M_* , the ratio $SFR(H\alpha)/SFR(FUV)$ grows by 0.5 dex. The smallest dispersion of this ratio, 0.298, is characteristic of the disks of spiral bulgeless galaxies which agrees with the concept of the decreasing role of star-formation bursts in the transition from dwarfs to massive galaxies.

Kaisin & Karachentsev (2014) imaged in the $H\alpha$ line a

hundred LV galaxies without known FUV fluxes. Based on the obtained data, $SFR(H\alpha)$ estimates for them can be converted to the $SFR(FUV)$ system via the empirical relation

$$\langle \log[SFR(H\alpha)/SFR(FUV)] \rangle = 0.16 \times \log M_* - 1.58.$$

On average, for Im and BCD galaxies, this relation yields a small correction equal to -0.20 dex, while for dIr galaxies, the correction is -0.40 dex. As seen from Fig. 9, data statistics for the E, S0, dSph- galaxies is so poor that it disallows any quantitative estimation.

When determining the $SFR(H\alpha)$ and $SFR(FUV)$ fluxes, we took into account the internal extinction in a galaxy:

$$A(H\alpha) = 0.54 \times A_B \quad \& \quad A(FUV) = 1.93 \times A_B,$$

where A_B is the extinction in the B band (in mag). According to Verheijen (2001), A_B can be expressed through the apparent axial ratio of a galaxy, a/b , and the rotation amplitude V_m (in km s^{-1}) as

$$A_B = [1.54 + 2.54(\log V_m - 2.2)] \log(a/b)$$

if $V_m > 40 \text{ km s}^{-1}$ and $A_B = 0$ for dwarfs with smaller rotation amplitude. Accounting for this relation, we built the diagrams of $\log[SFR(H\alpha)/SFR(FUV)]$ vs. $\log(a/b)$ for irregular galaxies ($T = 10, 9$), late-type ($T = 8-6$), and early-type ($T = 5-1$) spiral galaxies. The panels of Fig. 10 show the results, while the linear-regression parameters are given in the three last rows of Table 2. Dwarf irregular galaxies as well as early-type spirals do not exhibit any significant trend. But for the late-type spirals, such a trend is seen and described by the regression

$$\log[SFR(H\alpha)/SFR(FUV)] = -(0.24 \pm 0.11) \log(a/b) - 0.06.$$

Taking into consideration the relations between $A(H\alpha)$, $A(FUV)$, and A_B , we can conclude that the recipe from Verheijen (2001) overestimates the internal extinction in Scd, Sd, and Sm galaxies by the value $\Delta A_B = (0.43^m \pm 0.20^m) \log(a/b)$. Such a correction may be essential for thin edge-on galaxies.

7 MORPHOLOGICAL TYPE AND SURFACE BRIGHTNESS VS. ENVIRONMENT

The parameters considered above, M_{HI}/M_* and SFR/M_* , are rather sensitive to the environment density, since the light gaseous component of a galaxy is easily exposed to external influence. This is especially true for low-mass dwarf systems that dominate in the LV sample. Suppressing or intensifying star formation in a galaxy, the external influence affects also the morphological type and surface brightness of a galaxy.

Two panels of Fig. 11 show the dependence between the relative number of quenched E, S0, dSph- galaxies and the environment density parameters Θ_1 and Θ_j . The vertical bars correspond to the standard error of the mean. The bottom panel shows that among field galaxies with $\Theta_j < 1$, the fraction of passive galaxies is only 0–10 per cent, but in dense regions with $\Theta_j > 1$ their abundance sharply increases to 40–50 per cent. The top panel demonstrates a somewhat different pattern. The local density contrast Θ_1 from the most significant neighbour shapes a monotonous growth of

$f(E)$ from ~ 0 to ~ 50 per cent at $\Theta_1 < 2$. However, there is not any further growth seen at higher Θ_1 (possibly due to galaxy distance errors comparable to the virial radius of a group). Similar behaviour of a quenched fraction of satellites around the nearby luminous galaxies has been also noticed by Karachentsev & Kudrya (2015) and Fillingham et al. (2018).

As follows from the data in Fig. 12, the average surface brightness of galaxies within their Holmberg isophote in the B band varies by nearly one magnitude depending on the environment density. This effect is appreciably larger than statistical errors indicated by vertical bars. The average surface brightness is almost constant for field galaxies with $\Theta_j < 1$, while galaxies in groups with $\Theta_j > 1$ appear fainter, probably due to the presence of a considerable number of quenched spheroidal dwarfs. In the top diagram, the average surface brightness also drops with the growth of parameter Θ_1 , but it shows the reverse tendency with $\Theta_1 > 4$. Possibly this reversal is caused by tidal stripping of stellar periphery of companions located very closely to a massive neighbour. The SUCD1 ultra-compact companion near the massive Sombrero galaxy serves as an example.

Note, that theoretical predictions about the behaviour of surface brightness of galaxies in various environments are still rather sparse and vague. According to Hearin et al. (2017), ‘small galaxies cluster much more strongly than large galaxies of the same stellar mass’, but they have not found any quantitative estimate of this effect in terms of surface brightness.

8 CONCLUDING REMARKS

We have considered influence of an environment on global properties of galaxies: the neutral hydrogen abundance, star-formation rate, morphological type, and average surface brightness. The sample used contains 1029 galaxies within the sphere of 11 Mpc radius around the Milky Way. The bulk of this sample, ~ 85 per cent, is composed of dwarf galaxies most exposed to external action due to their shallow potential well.

To characterize an environment, we used two parameters: the density contrast Θ_1 provided by the most significant neighbour, and the local density excess Θ_j within 1-Mpc distance around a galaxy taken relative to the average cosmic density. Variations in the values of the parameters Θ_1 and Θ_j exceed five orders of magnitude. The hydrogen-to-stellar mass ratio of a galaxy reveals a weak effect of the H I deficiency in high-density regions being most noticeable in the case of low-mass irregular dwarfs.

The star-formation rate of the LV galaxies normalized to a unit of stellar mass turns out to be more sensitive to the environment density than M_{HI}/M_* ratio. Again, the fall of the specific star-formation rate with the growth of the environment density is most significant for the Ir, Im, and BCD dwarfs.

With a permanent present star-formation rate, dwarf galaxies and spiral galaxies without massive bulges are able to reproduce in average their observed stellar mass over the cosmological time $T_0 = 10.14$ dex (yr). Spiral galaxies of early types (Sa–Sb) and E, S0, dSph galaxies have the present sSFR able to reproduce only $\sim (1\text{--}10)$ per cent of

their stellar mass for the time T_0 . In other words, formation of stellar population in E, S0, and Sa galaxies has a significantly different (short and stormy) history than the sluggish process of converting gas into stars in irregular galaxies and spiral disks.

More than 99 per cent of the LV galaxies have a specific star-formation rate below -9.4 dex (yr^{-1}) i.e. below $5.5 \times H_0$. This critical threshold seems to be an important characteristic governing the evolution of the interstellar medium in the current epoch.

Comparison between the sSFRs determined from the H α and FUV fluxes shows a good mutual calibration for disks of spiral ($T = 1\text{--}8$) galaxies, being only slightly dependent on the environment. However, for dwarfs of the dIr and Im+BCD types, the average displacement of $\log[\text{SFR}(\text{H}\alpha)/\text{SFR}(\text{FUV})]$ is -0.40 dex and -0.20 dex, respectively. Also, the dispersion of this ratio significantly increases from spiral disks towards irregular dwarfs which is apparently indicative of star-formation bursts in dwarfs on a scale of $\sim 10^8$ yr (Skillman 2005, Stinson et al. 2007, Di Matteo et al. 2008).

The average $\text{SFR}(\text{H}\alpha)/\text{SFR}(\text{FUV})$ ratio decreases with the increase of apparent axial ratio of a galaxy which is especially noticeable for thin Scd–Sd–Sdm disks. This effect is evidently due to usual overestimation of the internal extinction in galaxy disks via the recipe by Verheijen (2001). For thin disks with the axial ratio $a/b = 10$, the extinction excess in the B-band amounts to $-0.43^m \pm 0.20^m$.

The abundance of quenched galaxies of the E, S0, dSph types grows from 0–10 per cent among field galaxies to 50 per cent in high-density regions, which is a demonstration of the well-known effect of the morphological segregation of galaxies. The average surface brightness of the LV galaxies also significantly varies with the environment density: dimmer galaxies without signs of star formation are more frequent in dense regions than in the general field. However, in the tight proximity of massive galaxies, one can see some indications of a competitive mechanism – stripping stellar periphery of dwarf companions by the tidal force from a massive neighbour.

Finally, we need to notice that about 20–40 per cent of the LV galaxies still do not have flux estimates both in the H I and in H α emission lines, and in the FUV band. Increasing the completeness of these surveys will allow one to take into consideration various effects of observational selection responsible for statistical biases more properly.

We thank the anonymous referee for numerous helpful comments that essentially improved the paper. This work is supported by the RSF grant no. 14–12–00965. The update of the database on LV galaxies is supported by the RFBR grant no. 18–02–00005.

REFERENCES

- Abramson L.E., Kelson D.D., Dressler A., et al. 2014, ApJ, 785L, 36
- Barsanti S., Owers M.S., Brough S., et al. 2018, ApJ, 857, 71
- Bell E.F., McIntosh D.H., Katz N., Weinberg M.D. 2003, ApJS, 149, 289
- Beygu B., Kreckel K., van der Hulst J.M., et al. 2016, MNRAS, 458, 394

- Binette L., Magris C.G., Stasinska G., Bruzual A.G., 1994, *A&A*, 292, 13
- Birrer S., Lilly S., Amara A. et al. 2014, *ApJ*, 793, 12
- Di Matteo P., Bournaud F., Martig M., et al. 2008, *A&A*, 492, 31
- Ellison S.L., Patton D.R., Simard L., McConnell A.W., 2008, *AJ*, 135, 1877
- Fillingham S.P., Cooper M.C., Boylan-Kolchin M., et al. 2018, arXiv:1802.03017
- Fingerhut R.L., McCall M.L., Argote M. et al., 2010, *ApJ*, 716, 792
- Fumagalli, M., Da Silva, R.L., & Krumholz, M.R. 2011, *ApJL*, 741, L25
- Gil de Paz A., et al., 2007, *ApJS*, 173, 185
- Hau G.K.T., Spitler L.R., Forbes D.A., et al. 2009, *MNRAS*, 394L, 97
- Haynes M.P., Giovanelli R., Martin A.M., et al. 2011, *AJ*, 142, 170
- Haynes M.P., Giovanelli R., 1984, *ARA & A*, 22, 445
- Hearin A., Behroozi P., Kravtsov A., Moster B., 2017, arXiv:1711.10500
- Huang S., Haynes M.P., Giovanelli R., et al. 2012, *AJ*, 143, 133
- Huchtmeier W.K., Karachentsev I.D., Karachentseva, V.E., Ehle M., 2000, *A&AS*, 141, 469
- Hunter D.A., Elmegreen B.G., & Ludka B.C. 2010, *AJ*, 139, 447
- James B.L., Kuposov S.E., Stark D.P., et al. 2017, *MNRAS*, 465, 3977
- Jarrett T.H., Chester T., Cutri R., Schneider S.E., Huchra J.P. 2003, *AJ*, 125, 525
- Jarrett T.N., Chester T., Cutri R. et al. 2000, *AJ*, 119, 2498
- Jones D.H., Peterson B.A., Colless M., Saunders, W., 2006, *MNRAS*, 369, 25
- Kaisin S.S., Karachentsev I.D., 2014, *Astrophys.Bull.*, 69, 390
- Kaisin E.I., Makarov D.I., Karachentsev, I.D., Kaisin S.S. 2012, *AstBu*, 67, 115
- Karachentsev I.D., Chengalur J.N., Tully R.B. et al. 2016, *AN*, 337, 306
- Karachentsev I.D., Kudrya Y.N., 2015, *AN*, 336, 409
- Karachentsev I.D., Kaisina E.I., Makarov D.I., 2014, *AJ*, 147, 13
- Karachentsev I.D., Makarov D.I., Kaisina E.I. 2013, *AJ*, 145, 101 (UNGC)
- Karachentsev I.D., Kaisina E.I., 2013, *AJ*, 146, 46
- Karachentsev, I.D., Karachentseva, V.E., Huchtmeier, W.K., Makarov, D.I. 2004, *AJ*, 127, 2031 (CNG)
- Karachentsev, I.D., 1994, *Astron.Astrophys.Trans.* 6,
- Kennicutt R.C., 1998, *ARA & A*, 36, 189
- Klypin A., Kravtsov A.V., Valenzuela O., & Prada F. 1999, *ApJ*, 522, 82
- Knapen J.H., Cisternas M., Querejeta M., 2015, *MNRAS*, 454, 1742
- Knobel C., Lilly S.J., Woo J., Kovac K., 2015, *ApJ*, 800, 24
- Koda J., Yagi M., Komiyama Y. et al. 2015, *ApJ*, 802L, 24
- Koribalski B.S., Staveley-Smith L., Kilborn V.A. et al. 2004, *AJ*, 128, 16
- Kovac K., Oosterloo T.A., van der Hulst J.M., 2009, *MNRAS*, 400, 743
- Kraan-Korteweg R.C. & Tammann G.A. 1979, *AN*, 300, 181
- Lee J.C., Veilleux S., McDonald M., Hilbert B., 2016, *ApJ*, 817, 177
- Lee J.C., Gil de Paz A., Kennicutt R.C., et al., 2011, *ApJS*, 192
- Lee J.C., Kennicutt R.C., Funes J.G., et al. 2009, *ApJ*, 692, 1305
- Lelli F., Verheijen M., Fraternali F., 2014, *MNRAS*, 445, 1694
- McGaugh S.S., Schombert J.M. 2014, *AJ*, 148, 77
- McQuinn K.B.W., Skillman E.D., Dolphin A.E., et al. 2016, *AJ*, 152, 144
- Meurer G.R., Wong O.I., Kim J.H., et al. 2009, *ApJ*, 695, 765
- Moore B., Ghigna S., Governato F., et al. 1999, *ApJ*, 524, L19
- Pan H.A., Lin L., Hsieh B.C., et al. 2018, arXiv:1801.04446
- Peebles P.J.E., 1993, *Principles of Physical Cosmology*, Princeton, University Press
- Pflamm-Altenburg J., Weidner C., & Kroupa P. 2009, *MNRAS*, 395, 394
- Pflamm-Altenburg J., Weidner C., & Kroupa P. 2007, *ApJ*, 671, 1550
- Pipino A., Calura F., Matteucci F., 2013, *MNRAS*, 432, 2541
- Ponomareva A.A., Verheijen M.A.W., Papastergis E., et al. 2018, *MNRAS*, 474, 4366
- Rodriguez-Puebla A., Primack J.R., Avila-Reese V., Faber S.M., 2017, *MNRAS*, 470, 651
- Sandage A., & Tammann G.A., Revised Shapley-Ames Catalog of Bright Galaxies, Carnegie Inst. of Washington, Publ. 635, 1981
- Schawinski K., Urry C.M., Brooke D.S., et al. 2014, *MNRAS*, 440, 889
- Schlafly E.F., & Finkbeiner D.P. 2011, *ApJ*, 737, 103
- Semenov V.A., Kravtsov A.V., Gnedin N.Y., 2017, *ApJ*, 845, 133
- Shimakawa R., Koyama Y., Prochaska J.X., et al. 2017, arXiv:1705.01127
- Skillman E.D., 2005, *NewAR*, 49, 453
- Stinson G.S., Dalcanton J.J., Quinn T. et al. 2007, *ApJ*, 667, 170
- Trinchieri G., de Serego Alighieri S., 1991, *AJ*, 101, 1647
- Vaduvescu O., Richer M.G., McCall M.L., 2006, *AJ*, 131, 1318
- Verheijen M.A.W., Sancisi R., 2001, *A & A*, 370, 765
- Warren B.E., Jerjen H., Koribalski B.S., 2004, *AJ*, 128, 1152
- Watkins A.E., Mihos J.C., Harding P., 2017, *ApJ*, 851, 51
- Weisz D.R., Johnson B.D., Johnson L.C., et al. 2012, *ApJ*, 744, 44

Table 1. Numbers of UNGC galaxies observed and detected in HI, FUV, H α .

Sample numbers	All types	T=10	T=9	T=8-6	T=5-1	T<1
UNGC (D<11.0,A<3.0)	1029	395	148	138	29	319
Observed in HI	794	329	127	130	29	179
Detected in HI	584	293	119	130	29	13
Observed in FUV	877	339	120	118	27	273
Detected in FUV	647	301	119	118	27	82
Observed in H α	573	228	89	117	29	110
Detected in H α	470	195	84	113	29	49
Detected both in HI and FUV or H α	557	276	111	127	29	12

Table 2. Linear regression parameters $Y = a + bX$ for the LV galaxies.

Y	X	T	N	$b \pm \sigma_b$	σ_Y	$\langle Y \rangle$	$\langle X \rangle$
$\log(M_{\text{HI}}/M_*)$	Θ_1	10	293	-0.060 \pm 0.020	0.475	-0.060	-0.043
$\log(M_{\text{HI}}/M_*)$	Θ_j	10	293	-0.025 \pm 0.016	0.479		0.033
$\log(M_{\text{HI}}/M_*)$	Θ_1	9	119	-0.016 \pm 0.040	0.494	-0.475	-0.211
$\log(M_{\text{HI}}/M_*)$	Θ_j	9	119	-0.015 \pm 0.026	0.493		0.004
$\log(M_{\text{HI}}/M_*)$	Θ_1	8-6	130	-0.020 \pm 0.027	0.439	-0.461	0.280
$\log(M_{\text{HI}}/M_*)$	Θ_j	8-6	130	-0.022 \pm 0.025	0.438		0.141
$\log(M_{\text{HI}}/M_*)$	Θ_1	5-1	29	0.024 \pm 0.092	0.603	-1.440	0.546
$\log(M_{\text{HI}}/M_*)$	Θ_j	5-1	29	-0.001 \pm 0.117	0.604		0.442
$\log(M_{\text{HI}}/M_*)$	Θ_1	<1	13	-0.229 \pm 0.152	0.907	-1.865	0.926
$\log(M_{\text{HI}}/M_*)$	Θ_j	<1	13	-0.256 \pm 0.152	0.888		0.554
$\log(\text{sSFR}_{\text{FUV}})$	Θ_1	10	301	-0.089 \pm 0.018	0.487	-10.239	0.356
$\log(\text{sSFR}_{\text{FUV}})$	Θ_j	10	301	-0.076 \pm 0.017	0.490		0.348
$\log(\text{sSFR}_{\text{FUV}})$	Θ_1	9	119	-0.105 \pm 0.033	0.380	-10.212	-0.163
$\log(\text{sSFR}_{\text{FUV}})$	Θ_j	9	119	-0.072 \pm 0.021	0.378		0.198
$\log(\text{sSFR}_{\text{FUV}})$	Θ_1	8-6	118	-0.002 \pm 0.024	0.381	-10.135	0.353
$\log(\text{sSFR}_{\text{FUV}})$	Θ_j	8-6	118	-0.051 \pm 0.025	0.374		0.241
$\log(\text{sSFR}_{\text{FUV}})$	Θ_1	5-1	27	0.084 \pm 0.092	0.600	-10.950	0.515
$\log(\text{sSFR}_{\text{FUV}})$	Θ_j	5-1	27	0.094 \pm 0.121	0.603		0.397
$\log(\text{sSFR}_{\text{FUV}})$	Θ_1	<1	82	-0.106 \pm 0.054	0.831	-12.227	1.856
$\log(\text{sSFR}_{\text{FUV}})$	Θ_j	<1	82	-0.152 \pm 0.082	0.833		1.293
$\log(\text{SFR}[\text{H}\alpha/\text{FUV}])$	Θ_1	10	161	0.054 \pm 0.030	0.535	-0.398	0.097
$\log(\text{SFR}[\text{H}\alpha/\text{FUV}])$	Θ_1	9	68	-0.081 \pm 0.052	0.461	-0.204	-0.240
$\log(\text{SFR}[\text{H}\alpha/\text{FUV}])$	Θ_1	8-6	98	0.018 \pm 0.021	0.300	-0.149	0.425
$\log(\text{SFR}[\text{H}\alpha/\text{FUV}])$	Θ_1	5-1	27	-0.085 \pm 0.047	0.308	0.118	0.515
$\log(\text{SFR}[\text{H}\alpha/\text{FUV}])$	Θ_1	<1	23	-0.268 \pm 0.085	0.696	0.011	1.700
$\log(\text{SFR}[\text{H}\alpha/\text{FUV}])$	Θ_j	10	161	-0.005 \pm 0.026	0.540	-0.398	0.220
$\log(\text{SFR}[\text{H}\alpha/\text{FUV}])$	Θ_j	9	68	-0.053 \pm 0.033	0.461	-0.204	-0.089
$\log(\text{SFR}[\text{H}\alpha/\text{FUV}])$	Θ_j	8-6	98	0.030 \pm 0.023	0.298	-0.149	0.318
$\log(\text{SFR}[\text{H}\alpha/\text{FUV}])$	Θ_j	5-1	27	-0.001 \pm 0.066	0.327	0.118	0.397
$\log(\text{SFR}[\text{H}\alpha/\text{FUV}])$	Θ_j	<1	23	-0.113 \pm 0.139	0.830	0.011	1.090
$\log(\text{SFR}[\text{H}\alpha/\text{FUV}])$	$\log(M_*)$	10	161	0.129 \pm 0.068	0.534	-0.398	7.463
$\log(\text{SFR}[\text{H}\alpha/\text{FUV}])$	$\log(M_*)$	9	68	0.142 \pm 0.102	0.463	-0.204	8.209
$\log(\text{SFR}[\text{H}\alpha/\text{FUV}])$	$\log(M_*)$	8-6	98	0.117 \pm 0.041	0.289	-0.149	9.143
$\log(\text{SFR}[\text{H}\alpha/\text{FUV}])$	$\log(M_*)$	5-1	27	-0.018 \pm 0.132	0.327	0.118	10.627
$\log(\text{SFR}[\text{H}\alpha/\text{FUV}])$	$\log(M_*)$	<1	23	0.074 \pm 0.102	0.832	0.011	8.173
$\log(\text{SFR}[\text{H}\alpha/\text{FUV}])$	$\log(a/b)$	10-9	229	-0.279 \pm 0.263	0.525	-0.340	0.220
$\log[\text{SFR}(\text{H}\alpha/\text{FUV})]$	$\log(a/b)$	8-6	98	-0.237 \pm 0.107	0.294	-0.149	0.382
$\log[\text{SFR}(\text{H}\alpha/\text{FUV})]$	$\log(a/b)$	5-1	27	-0.210 \pm 0.321	0.324	0.118	0.282

**APPENDIX A: LIST OF 1029 GALAXIES IN
THE LOCAL VOLUME WITH DISTANCE
ESTIMATES $D < 11.0$ MPC AND THE
GALACTIC B-BAND EXTINCTION $A_B < 3.0$
MAG.**

Name	RA (J2000.0) Dec.	T	D	log M^*	log(M_{HI})	log(SFR[FUV])	log(SFR[H α])	SB	Θ_1	Θ_j
UGC12894	000022.5+392944	10	8.47	7.58	7.92	-2.03	-2.29	25.2	-1.32	0.12
WLM	000158.1-152740	9	0.98	7.70	7.84	-2.23	-2.68	24.8	-0.04	1.75
And XVIII	000214.5+450520	-3	1.31	6.44	<6.65	< -5.84	< -5.97	26.8	0.54	1.54
PAndAS-03	000356.4+405319	-3	0.78	4.38		< -6.35		27.8	2.78	1.75
PAndAS-04	000442.9+472142	-3	0.78	5.59		-5.67	< -6.82	23.1	2.49	1.75
PAndAS-05	000524.1+435535	-3	0.78	4.75		< -6.38		25.6	2.77	1.75
ESO409-015	000531.8-280553	9	8.71	8.10	8.10	-1.72	-1.47	24.1	-1.98	-2.05
AGC748778	000634.4+153039	10	6.22	6.39	6.64	-3.53	-4.64	24.9	-1.87	-2.72
And XX	000730.7+350756	-3	0.80	5.26		-5.96	< -6.34	27.0	2.43	1.75
UGC00064	000744.0+405232	10	9.60	8.15	8.58	-1.63	-1.51	25.0	-1.88	-0.96
ESO349-031	000813.3-343442	10	3.21	7.12	7.13	-3.02	-4.03	24.7	0.15	1.75
NGC0024	000956.4-245748	5	7.31	9.48	8.64	-0.60	-1.01	24.5	-1.20	0.07

Notes. Morphological type in de Vaucouleurs scale, distance D in Mpc , stellar mass M^* and hydrogen mass M_{HI} in Solar mass units, SFR from FUV-flux and H α flux in (M_{sun}/yr), average B-band surface brightness in $mag/arcsec^2$, Θ_1 and Θ_j are dimensionless parameters characterizing the local density contrast.

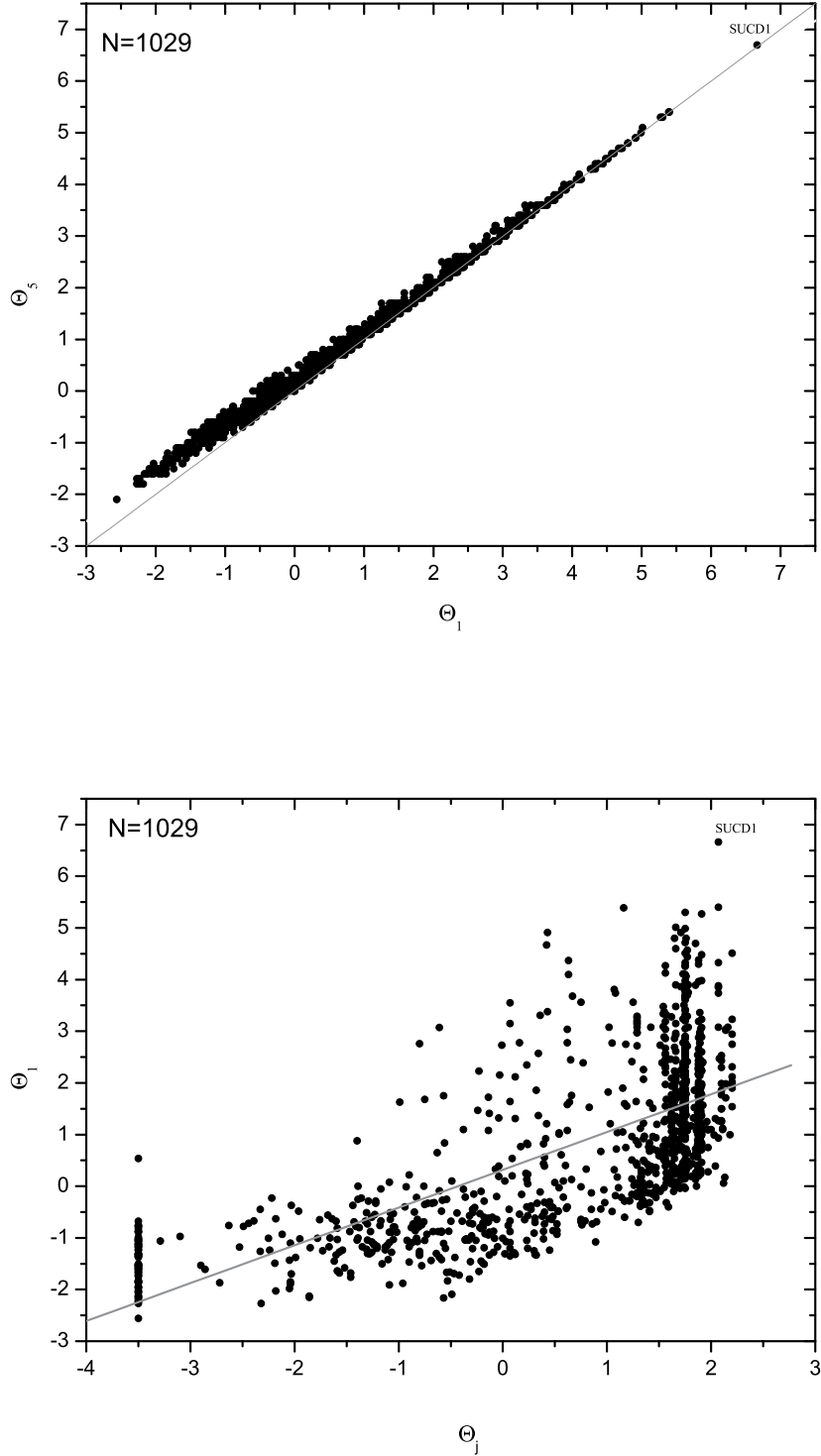


Figure 1. Comparison between three indices of the local density contrast. The upper panel – the tidal index determined by five significant neighbours versus the tidal index determined by the most significant neighbour. Lower panel – the tidal index determined by the most significant neighbour versus the local density contrast within 1 Mpc.

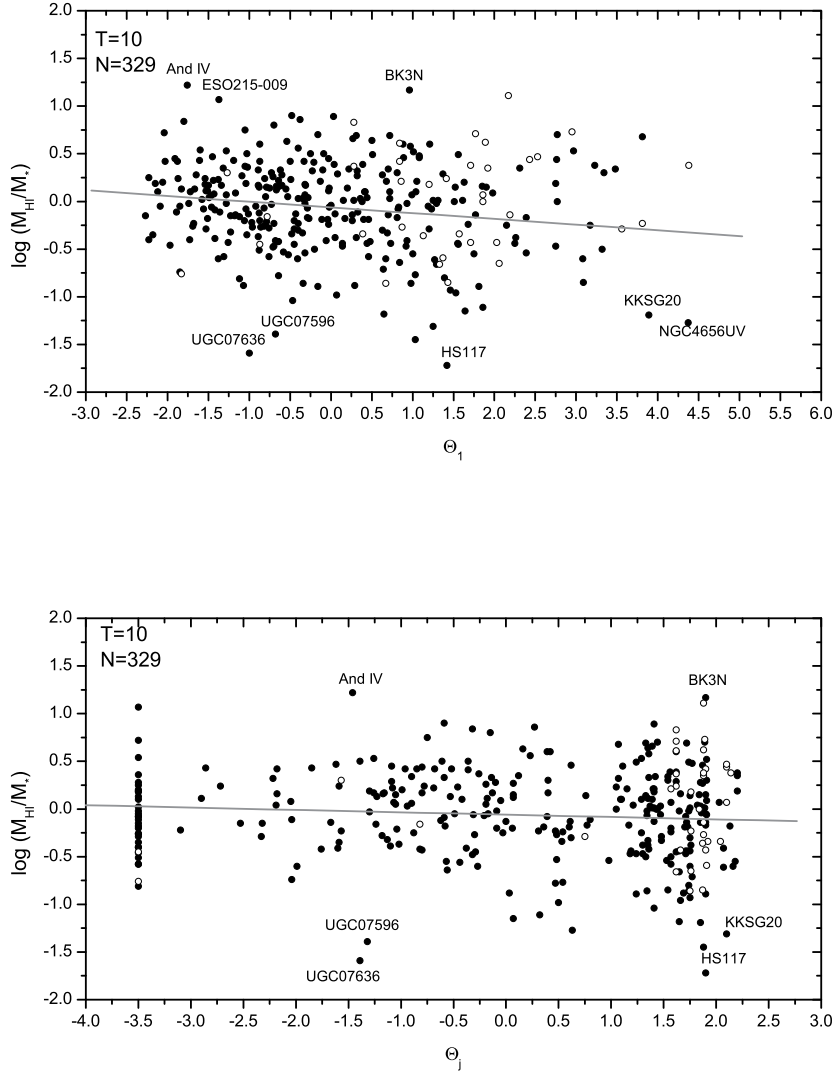


Figure 2. Hydrogen-to-stellar mass ratio as a function of the tidal index Θ_1 (the upper panel) and the local density contrast Θ_j (the lower panel) for dIrr ($T = 10$) galaxies. The galaxies with the upper limit of HI flux are shown by open circles. A typical uncertainty of the HI mass fraction on this and two next Figures is (0.1 - 0.2) dex.

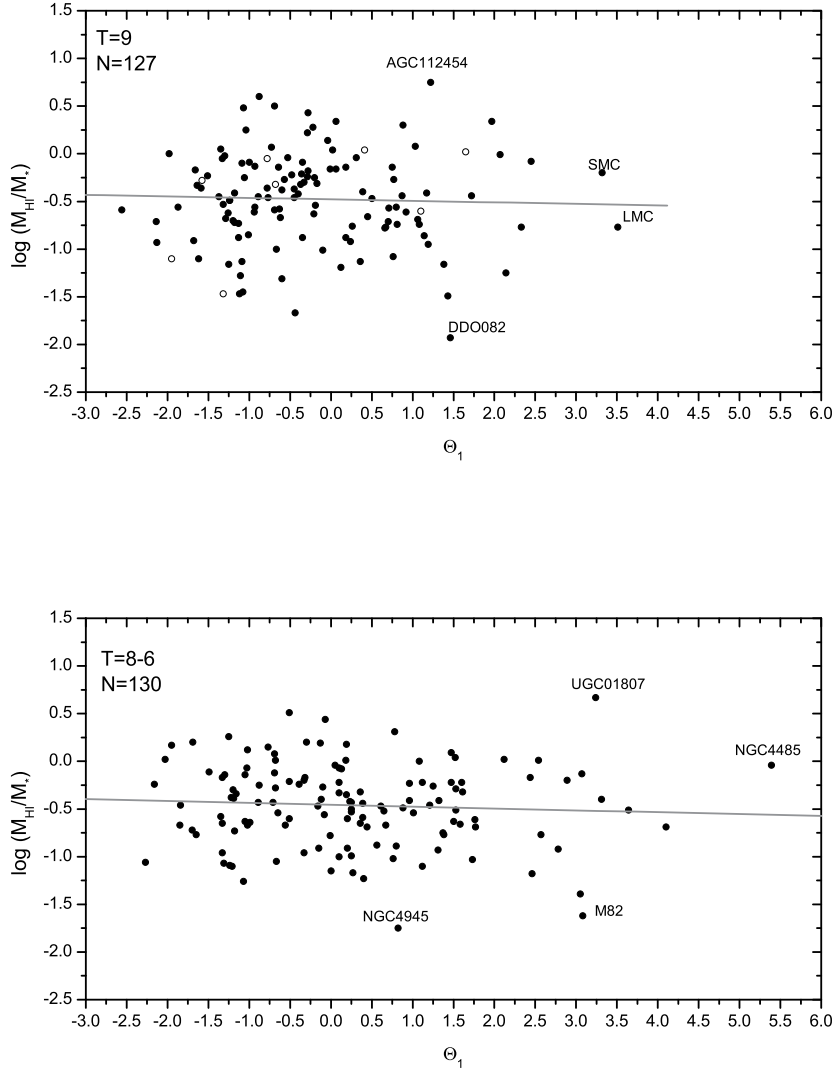


Figure 3. Hydrogen-to-stellar mass ratio as a function of the tidal index Θ_1 for Magellanic and Blue Compact Dwarfs ($T = 9$) (the upper panel) and for late-type spirals ($T = 8 - 6$) (the lower panel).

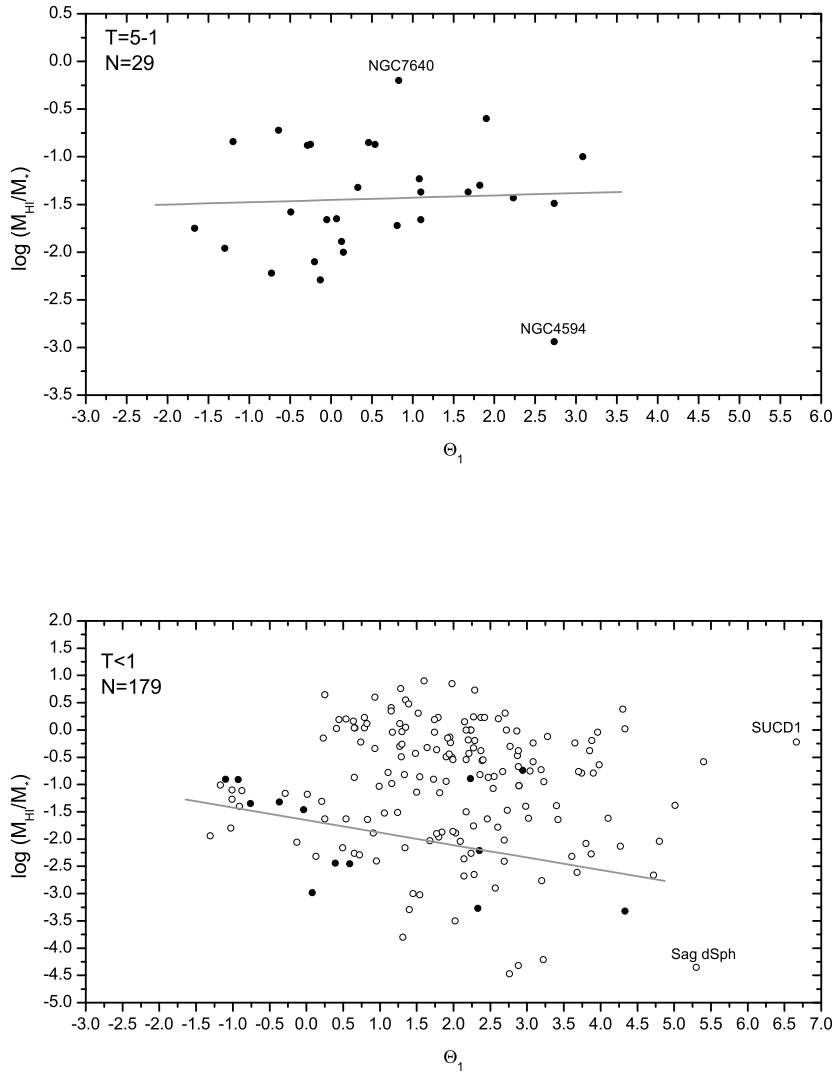


Figure 4. M_{HI}/M_* ratio as a function of Θ_1 for early-type spiral galaxies ($T = 5 - 1$) (the upper panel) and for E, S0, and dSph galaxies (the lower panel). The galaxies with the upper limit of H I flux are shown by open circles and not accounted for the regression line.

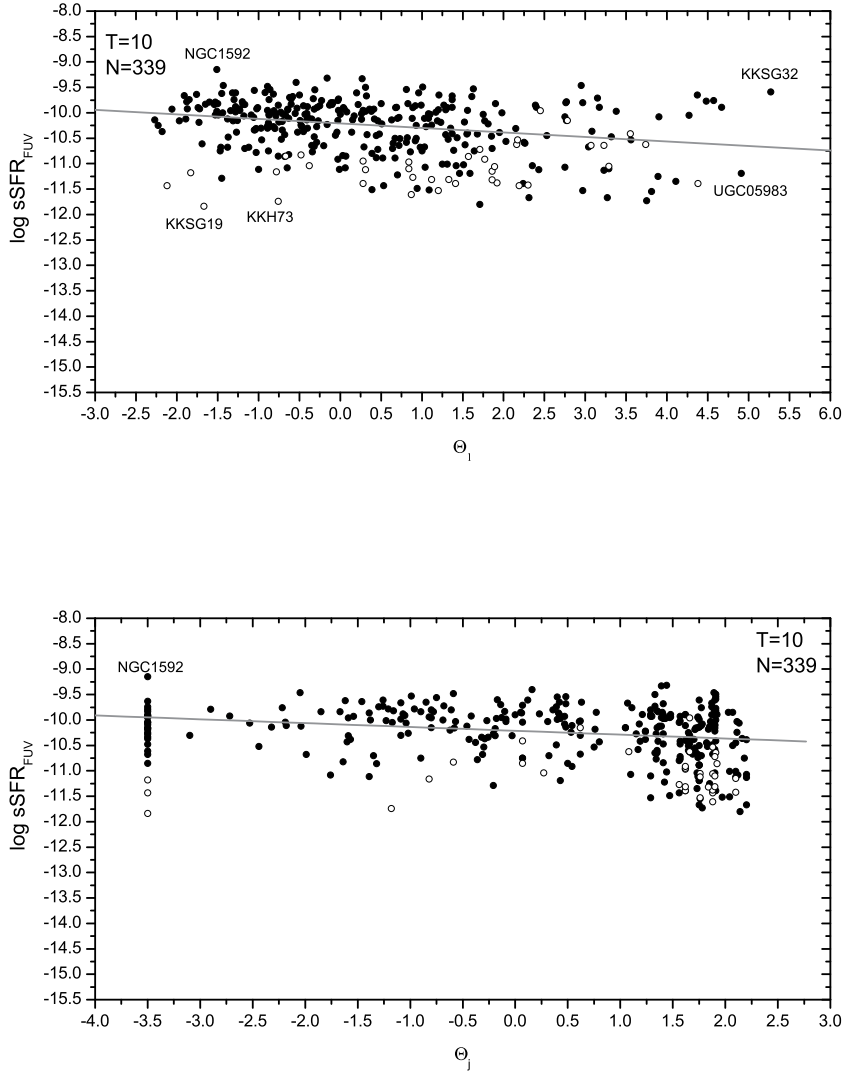


Figure 5. Specific star-formation rate versus Θ_1 (the upper panel) and Θ_j (the lower panel) for dIr galaxies. The galaxies with the upper FUV flux limit are shown by open circles. A typical uncertainty of sSFR on this and two next Figures is (0.1 - 0.2) dex.

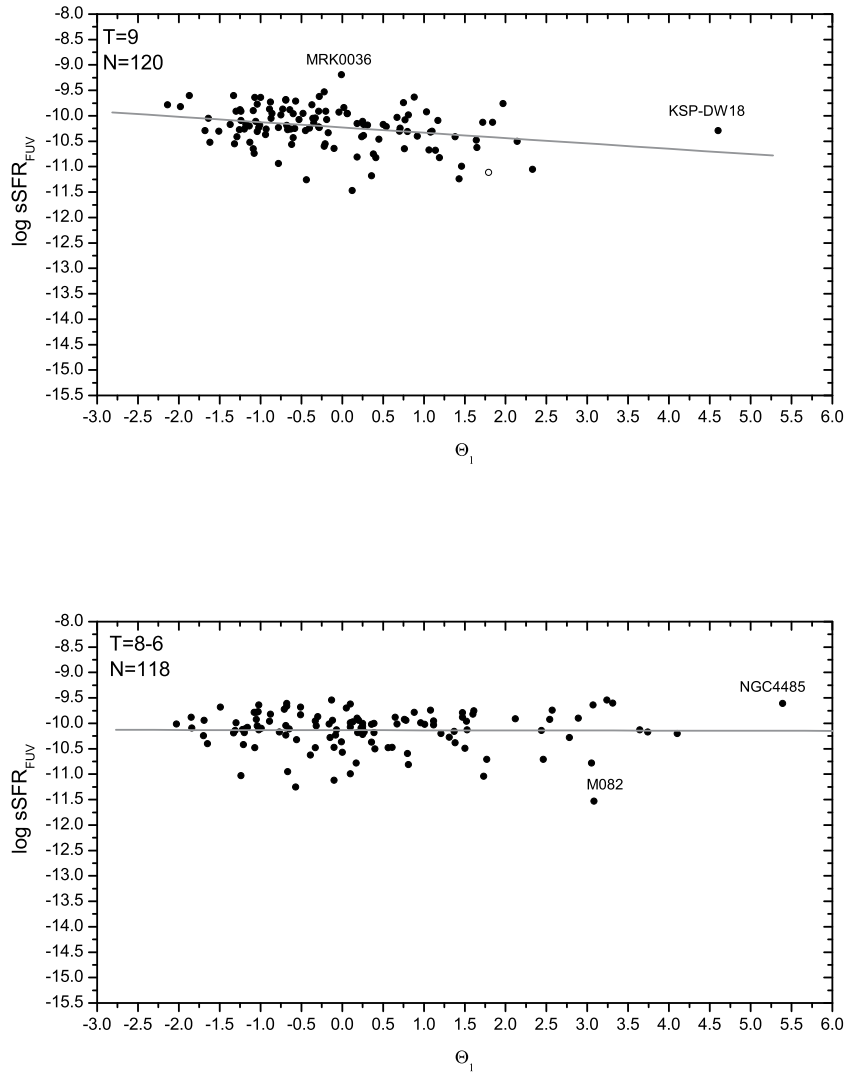


Figure 6. sSFR versus Θ_1 for Magellanic and Blue Compact Dwarfs (the upper panel) and for late-type spirals (the lower panel).

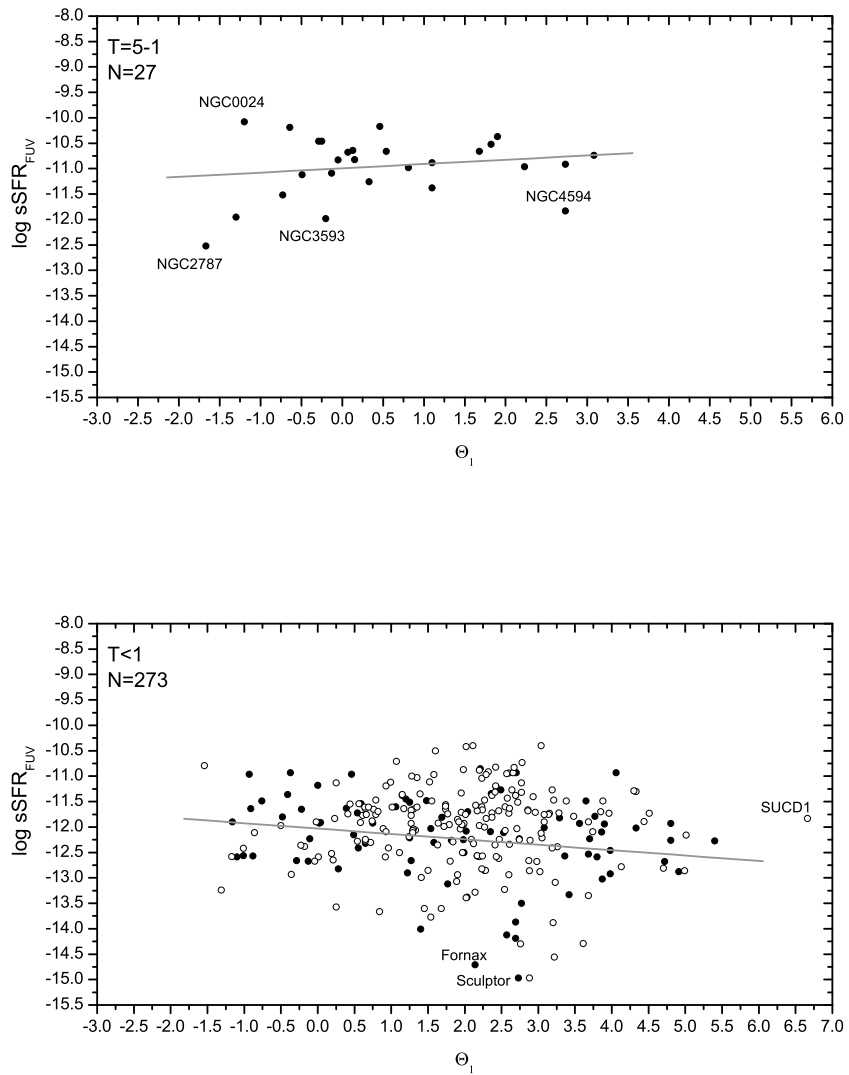


Figure 7. sSFR versus Θ_1 for early-type spiral galaxies (the upper panel) and for E, S0, and dSph galaxies (the lower panel).

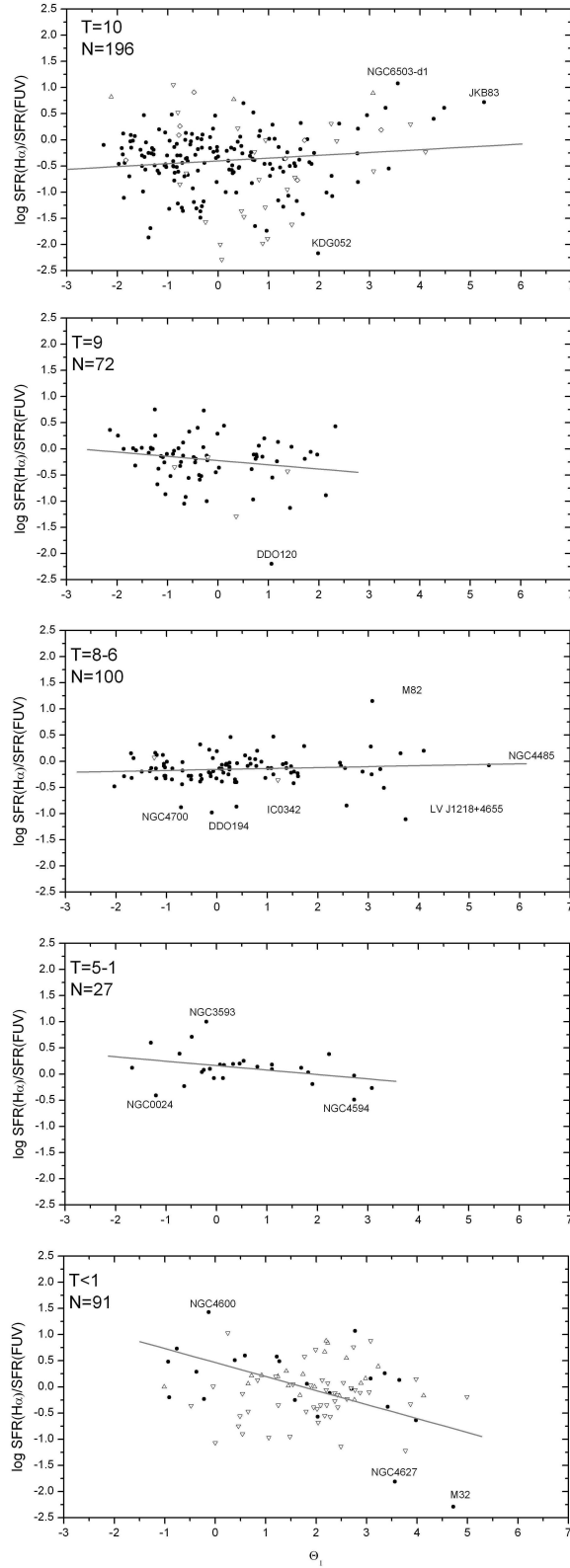


Figure 8. SFR ($\text{H}\alpha$)/SFR(FUV) versus Θ_1 for the LV galaxies of different morphological types. The galaxies with the upper limit to their $\text{H}\alpha$ or FUV flux are shown by point-down or point-up open triangles, respectively and not accounted for the regression line.

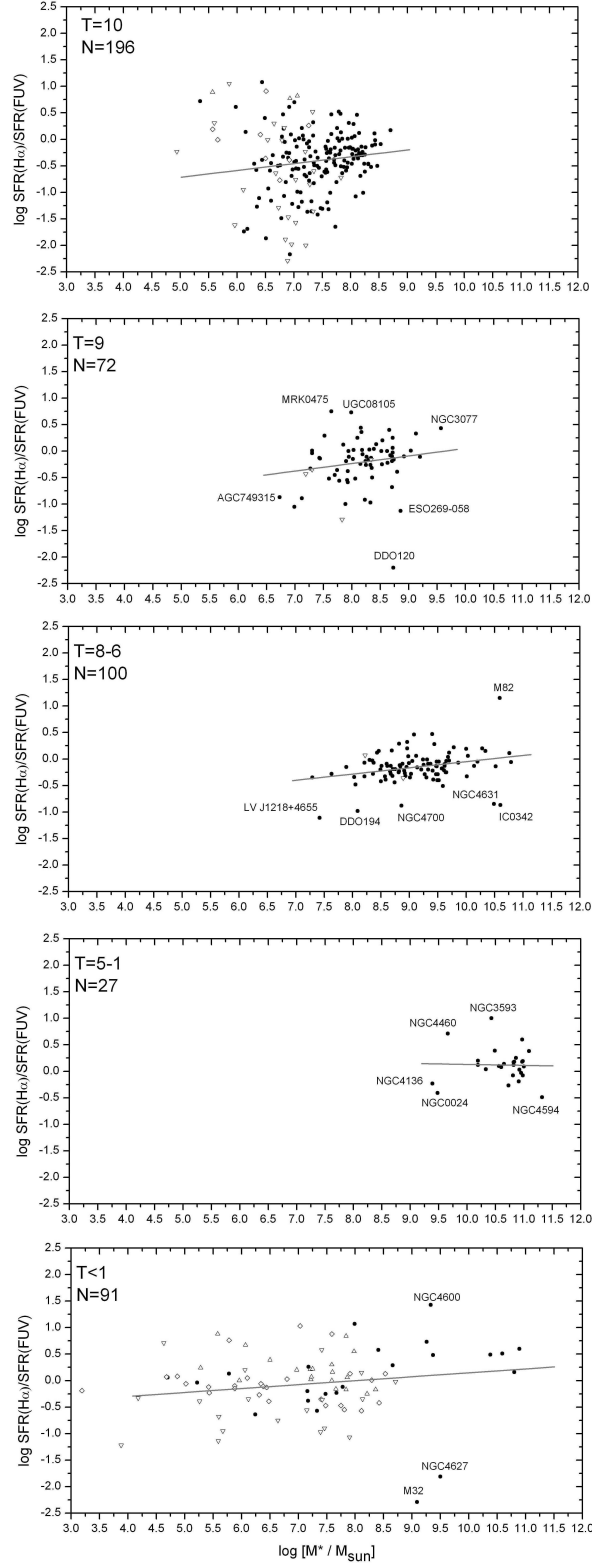


Figure 9. SFR ($\text{H}\alpha$)/SFR(FUV) versus the stellar mass for the LV galaxies of different morphological types. The galaxies with the upper limit to their $\text{H}\alpha$ or FUV flux are shown by point-down or point-up open triangles, respectively.

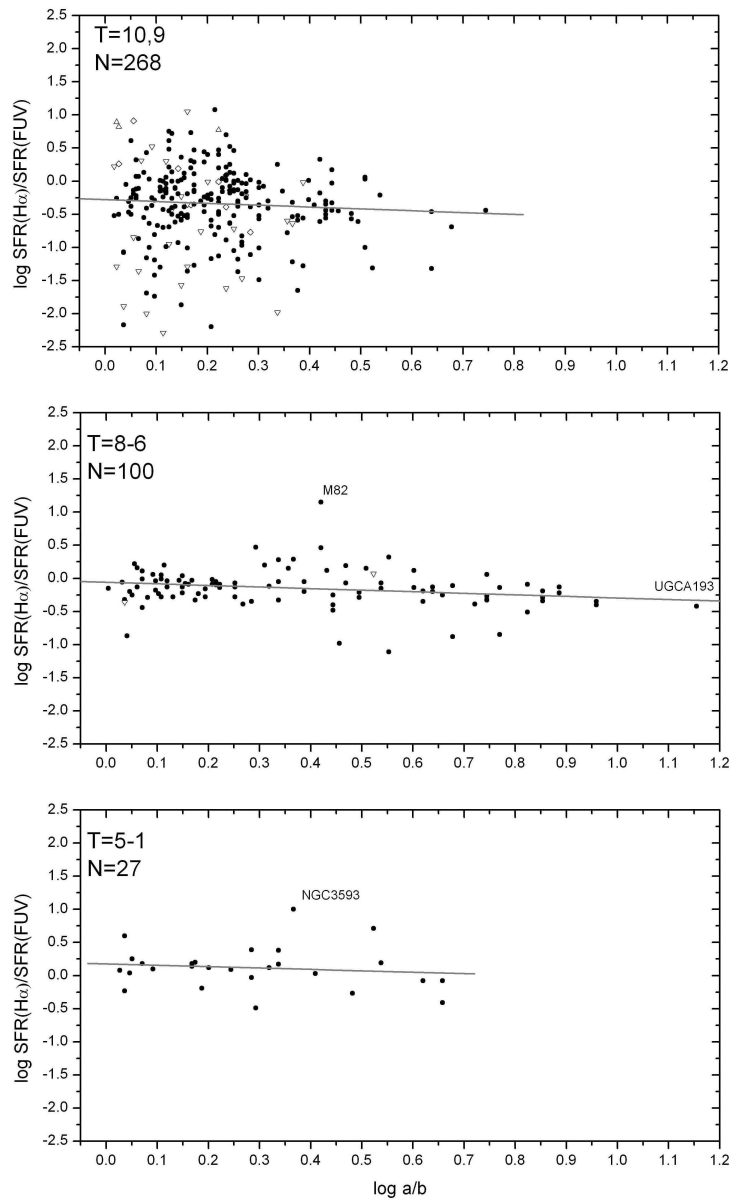


Figure 10. SFR ($\text{H}\alpha$)/SFR(FUV) versus the apparent axial ratio for the LV galaxies of dIr, dIm, and BCD types (the top panel), late-type spirals (the middle panel), and early-type spirals (the bottom panel).

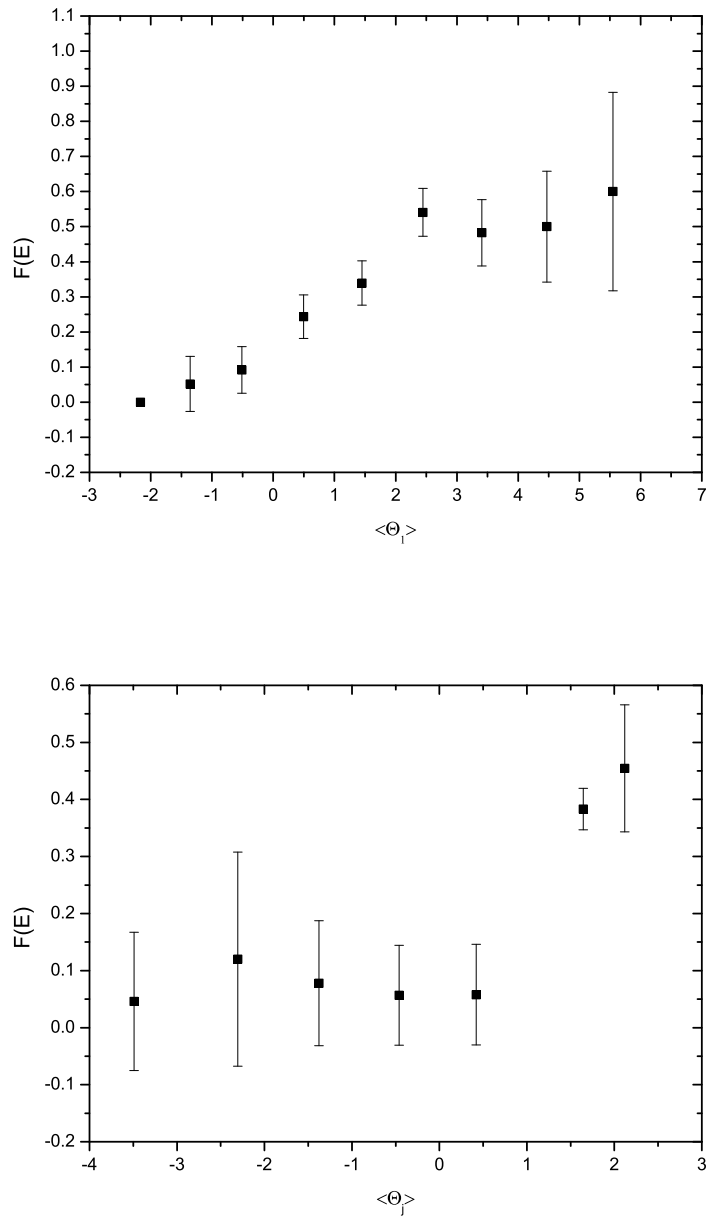


Figure 11. Fraction of (E, S0, dSph) galaxies versus the tidal index Θ_1 (the top panel) and the local density contrast Θ_j (the bottom panel). Vertical bars indicate standard errors.

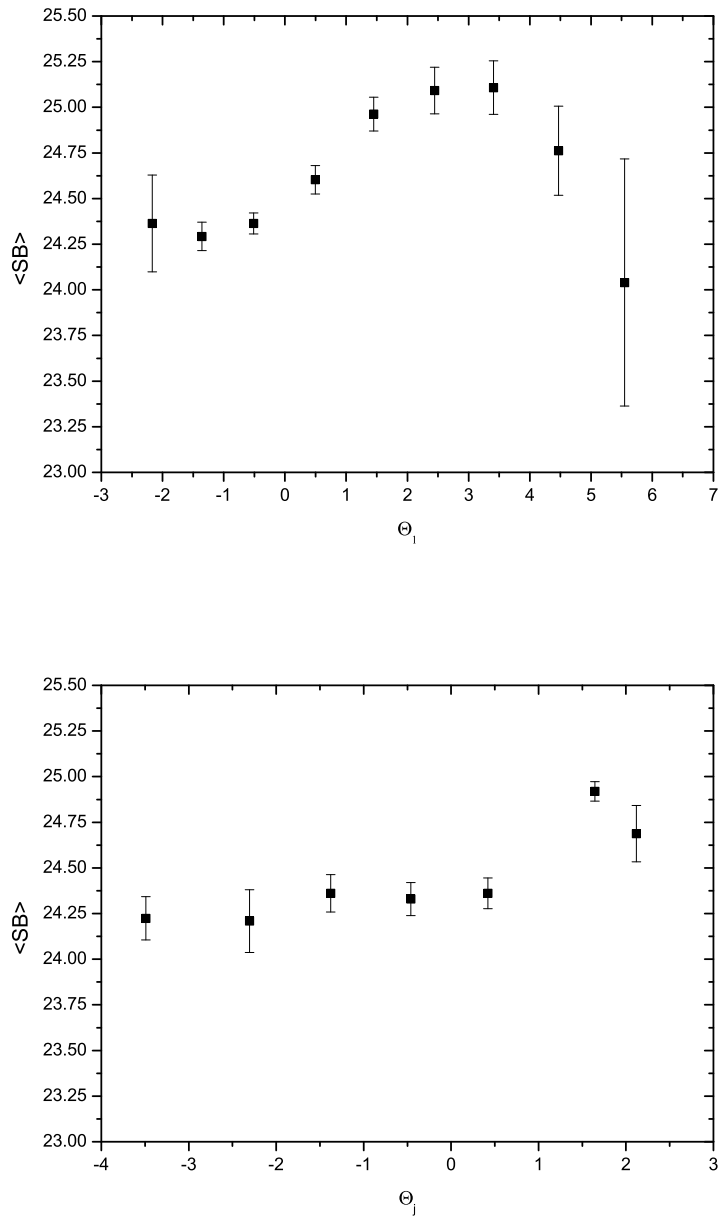


Figure 12. Mean surface brightness in the B band versus Θ_1 (the upper panel) and Θ_j (the lower panel). Vertical bars indicate standard errors.